Journal of Applied Polymer Science

Reactive Melt Blending of PS-POSS Hybrid Nanocomposites

O. Bianchi,[1,2] L. G. Barbosa,[1,3] G. Machado,[4] L. B. Canto,[5] R. S. Mauler,[1] R. V. B. Oliveira[1]

[1]Materials Science Graduate Program, Federal University of Rio Grande do Sul (UFRGS), Chemistry Institute (IQ), 91501-970 Porto Alegre, Rio Grande do Sul, Brazil

[2]University of Caxias do Sul, Caxias do Sul, Rio Grande do Sul, Brazil

[3]Federal Institute of Education, Science and Technology of Rio Grande do Sul, Campus Erechim (IFRS), Rio Grande do Sul, Brazil

[4]Center for Strategic Technologies of the North East (CETENE), Recife, Brazil

[5]Materials Engineering Department (DEMa), Federal University of São Carlos (UFSCar), 13565-905 São Carlos, Sao Paulo, Brazil

Correspondence to: R. V. B. Oliveira (E-mail: ricardo.oliveira@iq.ufrgs.br) or O. Bianchi (E-mail: otavio.bianchi@gmail.com)

ABSTRACT: Hybrid nanocomposites of polystyrene (PS) and methacryl phenyl polyhedral oligomeric silsesquioxane (POSS) were synthesized by reactive melt blending in the mixing chamber of a torque rheometer using dicumyl peroxide (DCP) as a free radical initiator and styrene monomer as a chain transfer agent. The effects of mixing intensity and composition on the molecular structure and morphology of the PS-POSS hybrid nanocomposites were investigated. The degree of POSS hybridization (α_{POSS}) was found to increase with the POSS content, DCP/POSS ratio, and rotor speed. For the PS-POSS materials processed in the absence of styrene monomer, an increase in the α_{POSS} led to a reduction in the molecular weight by PS chain scission, as a consequence of the free radical initiation. On the other hand, the use of styrene monomer as a chain transfer agent reduces the steric hindrance in the hybridization reaction between POSS and PS, enhancing the degree of POSS hybridization and avoiding PS degradation. The PS-POSS morphology consists of nanoscale POSS clusters and particles and microscale crystalline POSS aggregates. PS-POSS with higher α_{POSS} values and lower amounts of nonbound POSS showed improved POSS dispersion, characterized by smaller interfacial thickness (t) and greater Porod inhomogeneity lengths (l_p). The processing-molecular structure–morphology correlations analyzed in this study allow the POSS dispersion level in the PS-POSS materials to be tuned by controlling the reactive melt blending through the choice of the processing conditions. These insights are very useful for the development of PS-POSS materials with optimized performance. © 2012 Wiley Periodicals, Inc. J. Appl. Polym. Sci. 000: 000–000, 2012

KEYWORDS: PS; POSS; hybrid nanocomposite

Received 13 April 2012; accepted 13 June 2012; published online
DOI: 10.1002/app.38196

INTRODUCTION

Hybrid organic–inorganic nanocomposites have been used to impart new or improved properties to conventional polymers. These materials have become increasingly important in high-tech applications such as microelectronics and optics.[1,2] The performance of these materials is dependent on the chemical structure, shape, and size of the nanofillers, the degree of hybridization, and the dispersion, distribution, and interfacial adhesion between the nanofillers and the polymer matrix. Approaches to tailoring the structure and properties of these materials have focused on maximization of the surface to volume ratio of the nanofillers and the chemical interaction between these nanoparticles and the polymer matrix.[1,3–5]

Polyhedral oligomeric silsesquioxanes (POSS) have received considerable attention from the scientific community in the last few years because they possess a synergistic combination of properties of organic and inorganic materials.[6] POSS is comprised of inorganic/organic molecules, ~1–3 nm in size, and has the chemical formula $P_1R_7Si_8O_{12}$. It is composed of an inorganic silica-like core (Si_8O_{12}) surrounded by eight organic groups (P_1R_7). In most cases, R is an inert group, such as phenyl, cyclopentyl, isobutyl or methyl, and P is a reactive and/or a polymerizable functional group.[7] R groups are responsible for the high solubility of the POSS in organic solvents and polymer matrixes.[8] The use of POSS in copolymerization, grafting or even in blending through traditional processing methods can be applied to enhance polymer properties. Blending polymeric matrixes with POSS in the melt state[9–12] or in solution,[13] at low POSS percentages (2–5 wt %), leads to phase-separated materials with properties similar to or superior to the neat polymer. In contrast, hybridization of POSS onto polymeric chains has

Applied Polymer SCIENCE

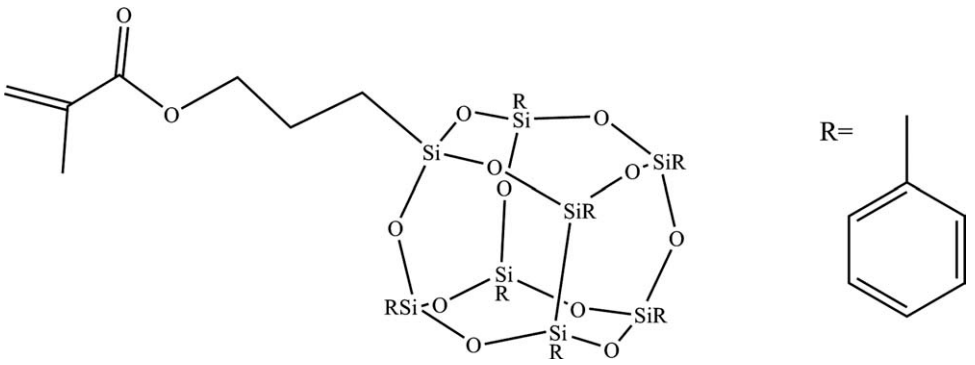

Figure 1. Chemical structure of methacryl phenyl POSS.

been shown to improve the POSS dispersion, leading to the enhancement of the flammability and the thermal and mechanical properties of conventional polymers. Polymerization at the *P* site, called *in situ* copolymerization, has been the most common approach used to produce hybrid polymer-POSS nanocomposites.[14–23] The use of reactive melt blending for POSS hybridization onto polymer backbones has become appealing because the process is environmentally friendly (free solvent) and economically viable[24,25] for the industrial development of POSS technology. In this context, Zhou et al. have studied the grafting of octavinyl-POSS onto PP chains initiated by peroxide.[26] They observed improved compatibility of POSS in the PP matrix, which was ascribed to partial POSS grafting onto PP chains. Monticelli et al. have studied the grafting of POSS onto polystyrene (PS) chains through the imidization reaction between amine-functionalized POSS (POSS-NH_2) and PS functionalized with maleic anhydride (PS-MAH). The resulting PS-POSS materials have shown POSS dispersion on the nanoscale, excellent transparency and increased hydrophobicity.[27] Many other studies have demonstrated the improved properties of PS-POSS hybrid nanocomposites.[1,13,15,28–30] However, the influence of the reactive melt blending conditions on the PS-POSS structure has been little explored.

In this study, PS-POSS hybrid nanocomposites were prepared by reactive melt blending of PS and POSS using dicumyl peroxide (DCP) as a free radical initiator and styrene monomer as a chain transfer agent. The melt processing was performed in the mixing chamber of a HAAKE torque rheometer under different processing conditions. The effects of mixing intensity and the amounts of POSS, DCP, and styrene monomer on the molecular structure and morphology of the PS-POSS hybrid nanocomposites were investigated in detail by size exclusion chromatography (SEC), NMR, synchrotron small-angle X-ray scattering (SAXS), wide angle X-ray diffraction (WAXD), scanning electron microscopy (SEM), transmission electron microscopy (TEM), and dynamic mechanical thermal analysis (DMTA). We provide some insights into how the molecular structure and morphology of PS-POSS hybrid nanocomposites, namely the degree of POSS hybridization, PS molecular weight and POSS dispersion level, can be tuned by controlling the reactive melt blending through the choice of the processing conditions. The observations reported herein provide a better understanding of the processing-molecular structure–morphology relationship, which are very useful in the development of PS-POSS materials with optimized performance. Moreover, they can be extended to other POSS-containing polymer systems.

EXPERIMENTAL

Materials

PS was purchased from Sigma-Aldrich under code 441147. It has a weight–average molecular weight (M_w) of 270,000 g mol^{-1} and a polydispersity (M_w/M_n) of 2, melt flow index (MFI) of 4 g 10^{-1} min^{-1} (200°C and 5 kg), and density of 1.05 g cm^{-3}. 3-(3,5,7,9,11,13,15-heptaphenylpentacyclo[9.5.1.$1^{3,9}$.$1^{5,15}$.$1^{7,13}$] octasiloxan-1-yl)propylmethacrylate (POSS®-(3-propylmethacrylate)) was purchased as a crystalline powder from Hybrid Plastics (USA) under code MA 0734a. It consists of T8 cages with the chemical structure shown in Figure 1. It has a molecular weight of 1083 g mol^{-1} and density of 1.25 g cm^{-3}. Styrene monomer (99.9% of purity) was purchase from Sigma-Aldrich under code 240869. DCP (98% of purity) was purchased from Sigma-Aldrich under code 329541. All chemicals were used as received.

Processing

PS-POSS hybrid nanocomposites containing 1, 2, and 5 wt % of POSS were prepared by reactive melt blending in the mixing chamber of a torque rheometer (Haake Rheomix 600p) with counter-rotating roller rotors, at a chamber temperature of 190°C for 15 min, at rotor speeds of 100, 150, and 200 rpm. DCP was used as a free radical initiator at different DCP/POSS ratios (0, 0.025, 0.05, 0.1, 0.2, 0.5, and 1 wt %). Styrene monomer was used as a chain transfer agent at a fixed amount of 2 wt %. The mixing protocols are summarized in Table I.

Materials were injection-molded as bars with dimensions of 40 × 12 × 3.2 mm^3 using an injection molding machine (Haake Minijet II) at a barrel temperature of 230°C, holding pressure of 500 bar and mold temperature of 30°C.

Size Exclusion Chromatography

SEC was used to determine the weight–average molecular weight (M_w) and the polidispersity (M_w/M_n) of the polymeric chains in PS-POSS hybrid nanocomposites. SEC analysis was performed using a Viscotek TDAmax™ chromatograph with triple detectors: differential viscosimeter (DV), light scattering (LS), and refractive index (RI). The following conditions were used: solvent tetrahydrofuran (THF), sample concentration 10 mg mL^{-1}, flow rate 1 mL min^{-1}, and sample volume 150 μL.

Table I. Mixing Protocols for Preparation of PS-POSS Hybrid Nanocomposites

POSS content (wt %)	Styrene content (wt %)	DCP/POSS (wt/wt %)	Rotor speed (rpm)
0, 1, 2, 5	-	0.05	100, 150, 200
2	-	0, 0.025, 0.05, 0.1, 0.2, 0.5, 1	200
0, 1, 2, 5	2	0.05	200

The column (Waters HR 4E, HR 4, HR 3, and HR 2) temperature was set at 45°C. The differential refractive index (d_n/d_c) used was 0.1850.[31] The analysis of the light scattering data by Viscotek software was carried out assuming that the second virial coefficient was zero.

Quantification of PS-POSS Reactions

The degree of POSS hybridization (α_{POSS}) in the PS-POSS hybrid nanocomposites was determined using size exclusion chromatography (SEC) and proton nuclear magnetic resonance (^{1}H NMR) spectroscopy through a calibration curve obtained from PS/POSS standards. The procedure is described in detail elsewhere.[32]

PS/POSS standards were prepared by solution casting. PS/POSS (1–20 wt % of POSS in PS) samples were dissolved in tetrahydrofuran (THF) at 5% w/v under mechanical stirring followed by ultrasonification for 6 h. Films were cast over glass plates and dried in a vacuum oven at 40°C for 48 h.

Solution ^{1}H NMR spectra were obtained in a VARIAN INOVA 300 instrument operating at 299.95 MHz. Samples were dissolved in $CDCl_3$ at 3% w/v. The analysis was performed at 22°C, using a spectral width of 10 ppm, acquisition time of 2.049 s, relaxation delay of 1 s and 128 scans. These measurements were performed to quantify the total amount of POSS in the PS/POSS standards and in the PS/POSS hybrid nanocomposites through the proton signal (4.2 ppm)[14,33] of the ester group present in POSS molecule (–O–CH_2) in relation to the aromatic proton signals (6.2–8 ppm) of the PS and POSS,[34] as shown in Figure 2(a).

SEC analysis was performed under the conditions described previously to quantify the amount of nonreacted POSS in the PS-POSS standards and in the PS-POSS hybrid nanocomposites through the POSS signal in the refractive index detector in the region of 33–38 min, as shown in Figure 2(b).

The calibration curve was constructed based on the POSS contents in the standards determined by ^{1}H NMR and SEC, as shown in Figure 2(c). Through this curve, the following relation was obtained:

$$\mathrm{POSS_{RMN}(mol\%)} = 0.9509 \cdot \mathrm{POSS_{SEC}(wt\%)}.$$

This curve provides the correlation between the POSS content data measured by SEC and by ^{1}H NMR.

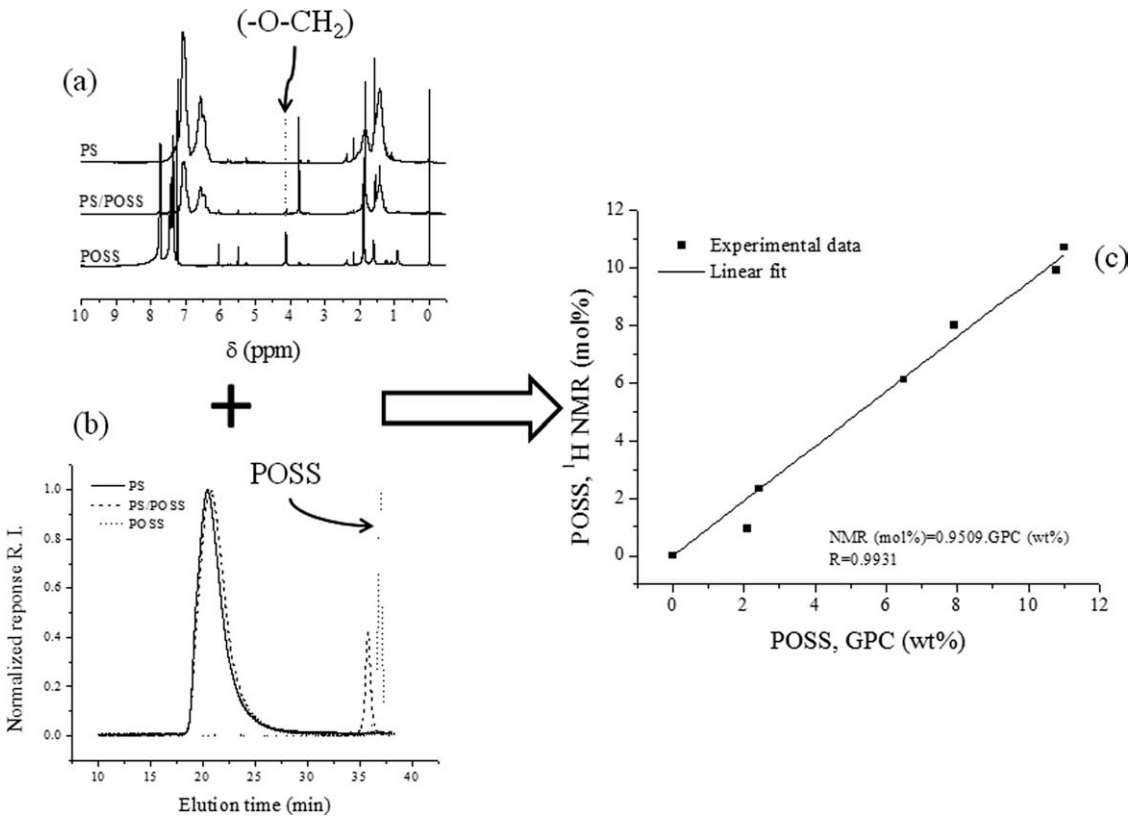

Figure 2. Method used for quantification of reaction in the PS-POSS hybrid nanocomposites. (a) ^{1}H NMR spectra, (b) Chromatographs of the SEC (refractive index detector), and (c) calibration curve.

The POSS hybridization degree (α_{POSS}) relative to the total POSS content in the PS-POSS hybrid nanocomposites was obtained through eq. (1):

$$\alpha_{POSS}(\%) = \frac{(POSS_{NMR}/0.9509) - POSS_{SEC}}{(POSS_{NMR}/0.9509)}.100 \quad (1)$$

where $POSS_{NMR}$ is the total amount of POSS present in each sample determined by ^{1}H NMR and $POSS_{SEC}$ is the quantity of unreacted POSS in each sample, which was determined by SEC measurements.

Scanning Electron Microscopy

The morphologies of the PS-POSS hybrid nanocomposites were examined using a JEOL JSM 6060 microscope equipped with an energy dispersive X-ray spectrometer (EDS). Samples from the central core of the injection-molded bars were cryo-fractured perpendicular to the mold filling. The tops of the fractured samples were sputter-coated with gold before SEM imaging.

Transmission Electron Microscopy

The morphologies of the PS-POSS hybrid nanocomposites were examined using a JEM-1200 EX II microscopy operated at an accelerating voltage of 80 kV. Samples from the central core of the injection-molded bars were cryo-fractured perpendicular to the mold filling. Thin sections (50 nm thick) were then microtomed at room temperature using a RMC PowerTome XL ultramicrotome equipped with a diamond knife. The thin sections were collected on 300-mesh copper TEM grids and stained in the vapor of OsO_4 (1 wt %) aqueous solution for 12 h for POSS contrast.

Synchrotron Small-Angle X-ray Scattering

SAXS experiments were performed at the SAXS1 beam-line of the Brazilian Synchrotron Light Laboratory (LNLS). An X-ray beam at a wavelength (λ) of 0.1488 nm was used. Incident photons were monitored and detected with a photomultiplier and marCCD 165 X-ray detector (8 × 8 binning). The exposure time was 50 s. Samples, with dimensions of 10 × 10 × 3.2 mm^3, were cut from the injection molded specimens. A sample-to-detector distance of 602 mm was used. Samples were placed with their surfaces perpendicular to the direction of the X-ray beam propagation and parallel to the X-ray detector. Scattering intensity (I) was measured as a function of scattering vectors (q) from 0.25 to 5.56 nm^{-1}. Background and parasitic scattering were determined using an empty holder and subtracted from each measurement.

SAXS Data Treatment

SAXS patterns are typically represented as scattered intensity (I) as a function of the magnitude of the scattering vector $q = 4\pi.\sin(\theta)/\lambda$, where 2θ is the angle between the incident X-ray beam and the detector, and λ is the wavelength of the X-rays.

In the case of a two-phase system, the only contrast leading to scattering in the typical range of resolution of the SAXS is the difference between the average electron densities ($\Delta\rho$) of the particle and the surroundings. The total integrated intensity of the SAXS pattern (in 3D) is an invariant quantity (Q) proportional to the $\Delta\rho^2$.

For an idealized two-phase system with a sharp interface, Porod's law states that the scattering intensity (I_{id}) decreases as a function of q^{-4} for large q (called the Porod region), with the proportionality constant related to the surface area (S) of the boundaries between two phases:[35,36]

$$\lim_{q\to\infty}[I_{id}(q)] = \frac{2\pi(\Delta\rho)^2 S}{q^4} \quad (2)$$

For an idealized two-phase system, the theoretical invariant (Q_{th}) is determined by eq. (3), where ϕ_1 and ϕ_2 are, respectively, the volume fractions of phases 1 and 2.[37,38]

$$Q_{th} = (\Delta\rho)^2\phi_1\phi_2 \quad (3)$$

The invariant can be determined experimentally (Q_{exp}) through eq. (4):

$$Q_{exp} = \frac{1}{2\pi^2}\int_{q_i^2}^{q_f^2} I(q)q^2\,dq \quad (4)$$

If the scattering intensity is determined in relative units, eq. (5) can be used to determine the surface to volume ratio or specific interfacial area (S/V):

$$\lim_{q\to\infty}\frac{I_{id}(q)q^4}{Q_{exp}} = \frac{2\pi S}{\phi_1\phi_2 V} \quad (5)$$

For an idealized two-phase system, the Porod inhomogeneity length (l_p) is given by eq. (6):

$$l_p = 4\pi\phi_1\phi_2\frac{V}{S} \quad (6)$$

As shown in eq. (6), l_p varies with the reciprocal of the specific interfacial area (S/V), that is, it is inversely proportional to the size of the domains. Physically, the Porod inhomogeneity length (l_p) is related to the average chord lengths of the phases.

A real two-phase polymer system shows deviations from Porod's law, that is, the product of $I(q)q^4$ does not give a constant value. A positive deviation is caused by the background scattering from the pure individual phases, which is due to the density fluctuations within the phases arising from thermal motions of the atoms.[39,40] The negative deviation is related to the existence of a diffuse transition region between two phases.[36]

The background scattering, $I_B(q)$, arising from thermal motions of the atoms within the phases can be matched according to the procedure proposed by Vonk et al. through the application of an empirical relation throughout the SAXS curve:[41–46]

$$I_B(q) = a + bq^n \quad (7)$$

The arbitrary constants a, b, and n (an even integer) in eq. (7) were found to match the SAXS curve at relatively high q values. The fitted curve is then extrapolated to smaller q values.

The scattered intensity in the Porod's region subtracted from the scattering background can be used to determine the interfacial thickness (t) and the specific interfacial area (S/V). In real two-phase materials with diffuse boundaries, eq. (2) can be modified according to eq. (8), where σ is the standard deviation of the Gaussian smoothing function:[36,41,45,47]

$$I(q) = I_{id}(q)e^{-\sigma^2 q^2} \quad (8)$$

In this study, eq. (8) was solved through the least squares method using the Levenberg-Marquardt algorithm.[48,49]

The Porod inhomogeneity length (l_p) can be obtained by replacing the solution of eq. (8) in eqs. (5) and (6).

The interfacial thickness (t) of the diffuse layer can be obtained from σ values by means of eq. (9)[36,50] considering a sigmoidal electron density profile:[40]

$$t = \sqrt{2\pi}\sigma \quad (9)$$

Wide Angle X-ray Diffraction

The crystalline structure of POSS in PS-POSS materials were characterized in a Siemens D500 diffractometer in the reflection mode using Cu Kα radiation (λ = 1.54 Å). The data were collected as a function of 2θ angle ranging from 1 to 40° at a scanning rate of 0.5 min^{-1}. The WAXD analysis of the POSS samples was performed using powder for PS and for the PS/POSS hybrid nanocomposite samples rectangular bars with dimensions of 40 × 12 × 3.2 mm^3 were used.

Dynamic Mechanical Thermal Analysis

The solid viscoelastic properties of the PS-POSS materials were measured in a DMA Q800 analyzer (TA Instruments) using a single cantilever geometry. Samples, rectangular bars with dimensions of 17 × 12 × 3.2 mm^3, were cut from the injection-molded specimens. The analysis was performed within the linear viscoelastic regime at small amplitude (0.1%), at a frequency of 1 Hz, in the temperature range of −100 to 150°C, at a heating rate of 3°C min^{-1}.

RESULTS AND DISCUSSION

PS-POSS Molecular Structure

PS-POSS hybrid nanocomposites were synthesized by reactive melt blending in the mixing chamber of a torque rheometer according to the processing conditions specified in Table I. Figure 3(a–d) shows a schematic representation of the chemical reactions that can occur during reactive melt blending of PS-POSS hybrid nanocomposites under the conditions adopted in this study. Thermal decomposition of DCP produces alkoxyl radicals that can abstract a hydrogen radical from the tertiary carbons of the PS backbone giving styryl macroradicals A (reaction pathway (a)). The macroradical A can react with methacryl-POSS in the presence of styrene monomer giving macroradical B (reaction pathway (b)). The macroradical B can react with a PS chain leading to the grafting of POSS onto the PS backbone (PS-graft-POSS) and giving another macroradical A (reaction pathway (c)). As styrene monomer is more reactive than POSS, it acts as a chain transfer agent reacting first with macroradical A and reducing the steric hindrance related to the insertion of the POSS into PS chain, thus maximizing the PS-POSS hybridization. Styrene monomer may also forms styryl radicals in the presence of DCP which can abstract hydrogen radicals from the PS backbone giving styryl macroradicals A, which are prone to decompose by β scission. Styrene monomer may also undergo polymerization in the presence of DCP. On the other hand, in the absence of styrene monomer, macroradical A can still react with methacryl-POSS; however, the steric hindrance in relation to the POSS insertion results in a lower degree of PS-POSS hybridization. Besides reacting with POSS or styrene, macroradical A can also decompose by β scission, giving a macroradical C and a PS chain with a terminal double bond, hence resulting in PS chain scission (reaction pathway (d)). This chain scission is favored when the monomer/initiator molar ratio is lower than 20, according to Passaglia et al.[21] Macroradical C can react with methacryl-POSS giving a macroradical D (reaction pathway (e)), which can react with a PS chain giving a POSS tethered at the end of the PS chain (PS-POSS) and giving another macroradical A (reaction pathway (f)). Briefly, the reactions for PS-POSS hybridization shown in pathway (f) are favored in the melt state because macroradicals of type C are less sterically hindered than those of type A.

Table II shows the PS-POSS torque and melt temperature responses during processing. For the PS-POSS hybrid nanocomposites processed without styrene monomer (chain transfer agent), the incorporation of increasing amounts of POSS reduced the processing torque level. This parameter appeared to have virtually no influence on the melt temperatures. The nanocomposites processed at higher rotor speeds (higher mixing intensity) showed lower mixing torques and higher melt temperatures. The nanocomposites processed with higher amounts of initiator (DCP/POSS ratio) showed lower processing torque levels. Once again, this parameter appeared to have virtually no influence on the melt temperatures. On the other hand, for the PS-POSS hybrid nanocomposites processed with styrene monomer as the chain transfer agent, the incorporation of increasing amounts of POSS increased the processing torque levels, with no influence on the melt temperature. Based on these data, we can infer that the processing conditions, namely the mixing intensity and the amounts of POSS, initiator (DCP) and chain transfer agent (styrene monomer), affect the molecular structure of PS-POSS hybrid nanocomposites. This will be discussed below.

The efficiency of the POSS hybridization in relation to the POSS content, given by α_{POSS} [eq. (1)], the relative amounts of nonreacted and hybridized POSS and the weight–average molecular weights (M_w) of the PS-POSS nanocomposites were determined as a function of the processing conditions. The data obtained are shown in the plots of Figures 4–6. Curves were drawn by connecting the data points in order to facilitate the visualization.

In order to investigate the effects of the rotor speed (mixing intensity) and POSS content added on these structural parameters, the PS-POSS nanocomposites containing 0–5 wt % of POSS were processed with a fixed amount of initiator (DCP/

Applied Polymer SCIENCE

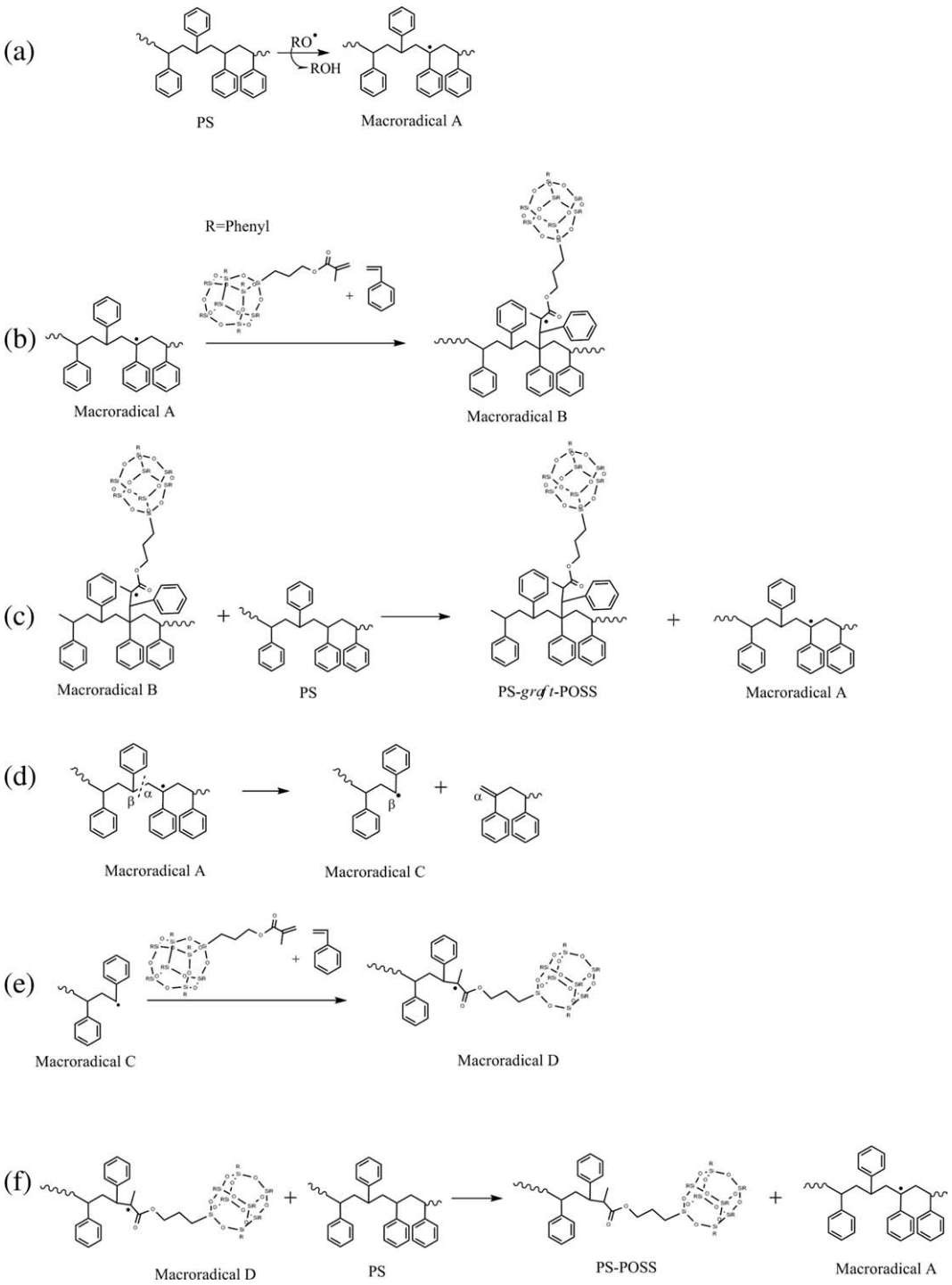

Figure 3. Schematic representation of the chemical reactions that may occur during reactive melt blending of PS-POSS hybrid nanocomposites. (a) Styryl macroradical formation, (b) PS-graft-POSS macroradical formation, (c) PS-graft-POSS formation, (d) PS chain scission, (e) PS-end-chain-POSS macroradical formation, and (f) PS-end-chain-POSS formation.

POSS = 0.05) at rotor speeds of 100, 150, and 200 rpm, without chain transfer agent (styrene monomer). The results are shown in Figure 4(a–c). The degree of POSS hybridization (α_{POSS}) [Figure 4(a)], and thus the relative amounts of hybridized POSS [Figure 4(b)], increased with POSS content in the PS-POSS nanocomposites. It is important to note that the increase in the amount of POSS added is accompanied by increased DCP contents in relation to PS, since the DCP/POSS ratio was kept constant in the processing. Hence, the increase in the POSS and thus in the DCP available leads to a higher number of reactive sites being available for the hybridization reaction, resulting in increased α_{POSS} values. On the other hand, the

Table II. Torque and Melt Temperature Responses for PS-POSS Hybrid Nanocomposites Melt Blended in the Torque Rheometer Under Different Processing Conditions

PS/POSS (wt/wt %)	Styrene content (wt %)	DCP/POSS (wt/wt %)	Rotor speed (rpm)	Torque (Nm)[a]	Melt temperature (°C)[b]
100/0	-	0.05	100	6.7 ± 0.1	201.1 ± 0.1
99/1				6.1 ± 0.1	200.5 ± 0.1
98/2				5.5 ± 0.1	201.7 ± 0.1
95/5				5.8 ± 0.1	201.9 ± 0.1
100/0	-	0.05	150	5.7 ± 0.1	206.7 ± 0.1
99/1				5.6 ± 0.1	206.1 ± 0.1
98/2				5.1 ± 0.1	205.9 ± 0.1
95/5				5.4 ± 0.1	205.3 ± 0.1
100/0	-	0.05	200	5.1 ± 0.1	210.2 ± 0.1
99/1		0.05		5.1 ± 0.1	209.4 ± 0.1
98/2		-		5.1 ± 0.1	210.8 ± 0.1
98/2		0.025		5.1 ± 0.1	210.4 ± 0.1
98/2		0.05		5.0 ± 0.1	209.6 ± 0.1
98/2		0.1		5.0 ± 0.1	209.8 ± 0.1
98/2		0.2		5.0 ± 0.1	209.6 ± 0.1
98/2		0.5		4.8 ± 0.1	209.4 ± 0.1
98/2		1		4.8 ± 0.1	209.7 ±0.1
95/5		0.05		4.8 ± 0.1	208.5 ± 0.1
100/0	2.0	0.05	200	4.7 ± 0.1	209.1 ± 0.1
99/1				5.4 ± 0.1	210.6 ± 0.1
98/2				5.1 ± 0.1	210.3 ± 0.1
95/5				5.4 ± 0.1	210.1 ± 0.1

[a]Stabilized torque values taken at 14–15 min of mixture, [b]Average melt temperature taken at 14–15 min of mixture.

increase in the DCP available leads to a reduction in the M_w [Figure 4(b)] due to PS chain scission. Briefly, for PS-POSS nanocomposites processed without styrene monomer the increase in α_{POSS} occurs at the expense of decreased molecular weight, that is, PS chain scission occurs simultaneously with POSS hybridization during the reactive melt blending, according to the reaction scheme shown in Figure 3. PS-POSS nanocomposites processed at higher mixing intensity (high rotor speed) showed higher α_{POSS} [Figure 4(a)] and thus higher relative amounts of hybridized POSS [Figure 4(b)] and lower M_w values [Figure 4(c)]. This behavior is due to the greater amount of energy supplied during processing performed at higher rotor speeds, which increases the degree of POSS hybridization and enhances the PS chain scission.

This increase in the POSS hybridization with simultaneous PS chain degradation on increasing the content of POSS and/or rotor speed during the melt processing of PS-POSS nanocomposites explains the decrease in the processing torque (Table I). The increase in the rotor speed leads to a higher shear rate during the mixing which, in addition to the higher degree of hybridization achieved, results in greater heat generation. Both effects contribute to a rise in the melt temperature causing melt thinning which decreases the mixing torque (Table I).

The dependence of the degree of POSS hybridization (α_{POSS}), relative amounts of nonreacted and hybridized POSS and weight–average molecular weight (M_w) on the amount of initiator (DCP) was investigated for PS-POSS hybrid nanocomposites with 2 wt % of POSS processed at a rotor speed of 200 rpm, without chain transfer agent (styrene monomer). The results are shown in Figure 5(a–c). The increase in the amount of DCP initiator in relation to POSS, given by the DCP/POSS ratio, increased the α_{POSS} value [Figure 5(a)] and thus the relative amount of hybridized POSS [Figure 5(b)] in the PS-POSS nanocomposites; however, it reduced the M_w values [Figure 5(c)]. The increase in the amount of DCP resulted in a greater amount of A-type macroradicals which increases the PS-POSS hybridization. However, it also intensifies the PS chain scission, according to the reaction scheme shown in Figure 3. A reduction in the molecular weight is commonly observed in the chemical modification of polymers initiated by free radicals, as in the modification of polypropylene (PP) with maleic anhydride (MAH)[51] and vinyltriethoxysilane.[52]

The reduction in the molecular weight in the PS-POSS processed with increasing amounts of DCP explains the decrease in the processing torque (Table I).

Applied Polymer SCIENCE

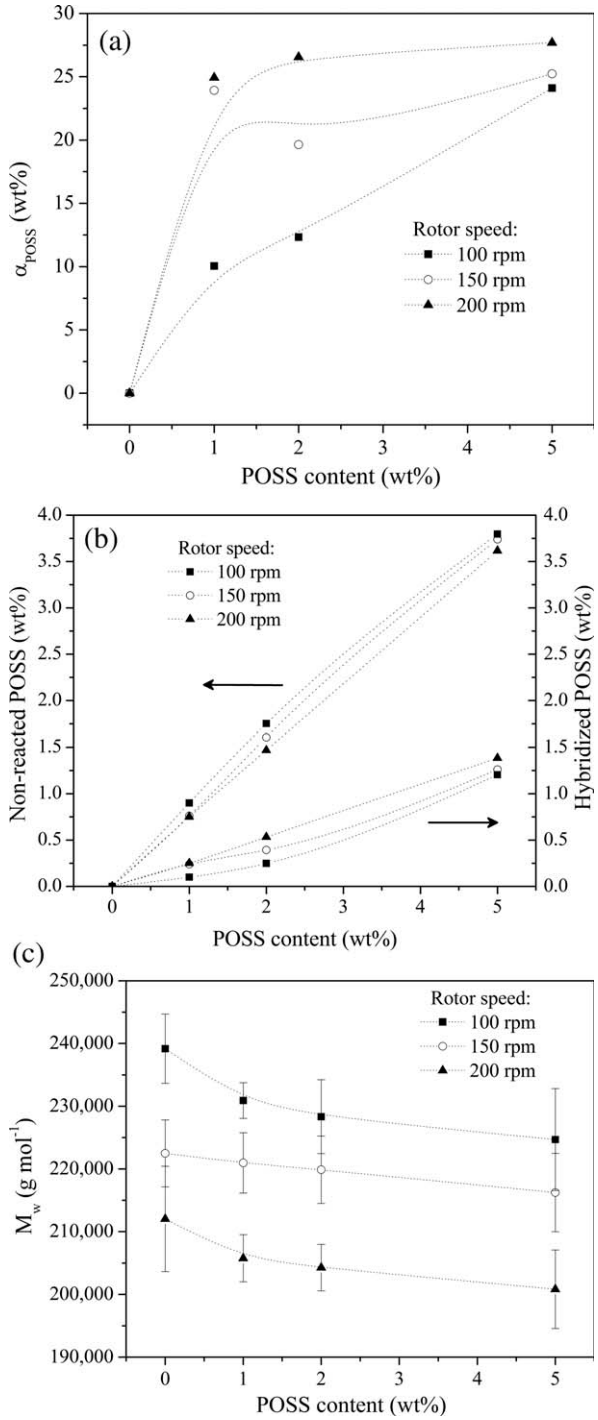

Figure 4. Effects of POSS content added and rotor speed (mixing intensity) on POSS hybridization degree (α_{POSS}) (a), relative amounts of nonreacted and hybridized POSS (b), and weight–average molecular weight (M_w) (c) for PS/POSS hybrid nanocomposites processed with DCP/POSS = 0.05 without styrene monomer.

The dependence of α_{POSS}, the relative amounts of nonreacted and hybridized POSS and the weight–average molecular weight (M_w) on the styrene monomer addition in the reactive melt processing of PS-POSS nanocomposites was investigated for a series of nanocomposites containing 1–5 wt % of POSS, processed with a fixed amount of initiator (DCP/POSS = 0.05) at a rotor speed of 200 rpm. The results are shown in Figure 6(a–c). The use of 2 wt % of styrene monomer in the synthesis of PS-POSS nanocomposites increased the α_{POSS} value [Figure 6(a)]

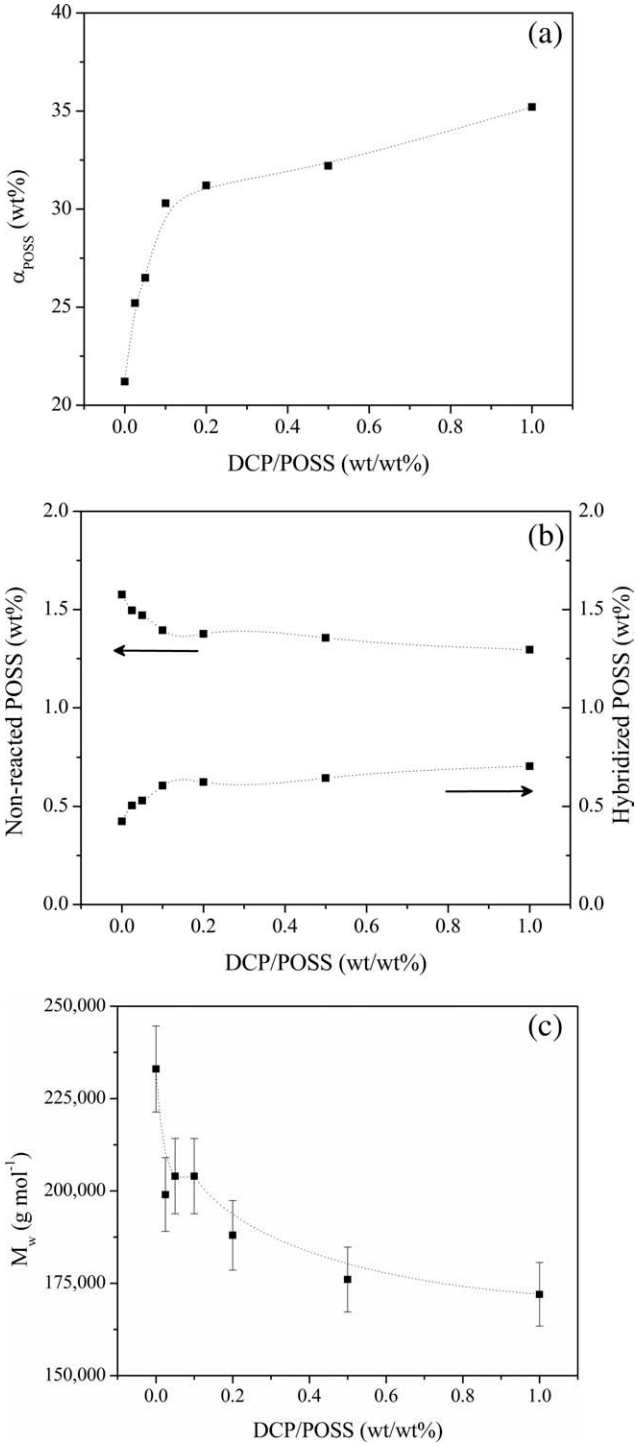

Figure 5. Effects of DCP/POSS ratio on (a) αPOSS value, (b) relative amounts of nonreacted and hybridized POSS, and (c) M_w for a series of PS-POSS 98/2 hybrid nanocomposites processed in a torque rheometer (200 rpm).

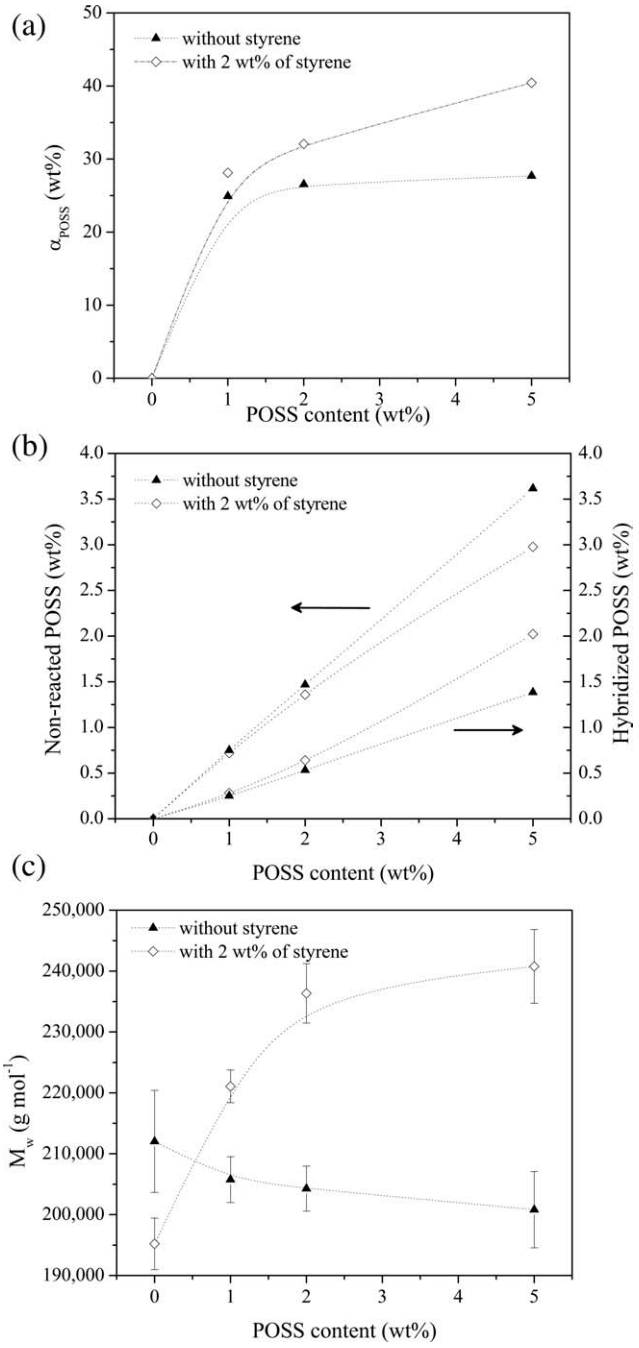

Figure 6. The effects of the use of styrene monomer as a chain transfer agent on (a) αPOSS value, (b) relative amounts of nonreacted and hybridized POSS, and (c) M_w for a series of PS-POSS hybrid nanocomposites with different amounts of POSS (DCP/POSS = 0.05) processed in a torque rheometer (200 rpm).

and thus the relative amounts of hybridized POSS [Figure 6(b)] when compared with analogous PS-POSS nanocomposites melt processed in the absence of styrene monomer. Styrene monomer acts as a chain transfer agent reducing the steric hindrance in relation to the insertion of POSS into the PS chain, hence maximizing the PS-POSS hybridization reaction, as shown in the reaction scheme of Figure 3.

The degrees of PS-POSS hybridization achieved in this study (up to 40 wt %) are comparable to those obtained in other POSS-containing polymer systems prepared through reactive melt processing via free radical initiation. For instance, Zhou et al.[26] reached up to 50% of grafting in a PP-POSS system. Using another experimental approach, Monticelli et al.[27] reached up to 90 wt % of grafting in PS-POSS materials obtained by reactive processing through an imidization reaction between amine functionalized POSS (POSS-NH_2) and PS functionalized with maleic anhydride (PS-MAH). Whatever the POSS-polymer system, the authors are unanimous in attributing the difficulty associated with POSS-polymer hybridization to the steric bulkiness and self-aggregation of POSS particles even when added in small quantities to the polymer matrix.[22,53,54] This aspect will be discussed below.

Another notable feature in the plots of Figure 6(a–c) is that the increase in αPOSS values [Figure 6(a)] was accompanied by an increase in the molecular weight (M_w) [Figure 6(c)] for the PS-POSS hybrid nanocomposites processed in the presence of styrene monomer as a chain transfer agent, unlike the analogous PS-POSS processed in the absence of styrene monomer (Figure 4). For neat PS (0% of POSS), however, the use of styrene monomer during melt processing reduced the molecular weight. When neat PS is melt processed in the presence of both DCP and styrene monomer, a larger number of A-type macroradicals prone to undergo β-chain scission are formed, compared with the neat PS processed with only DCP. This is because the styrene monomer in the presence of DCP forms styryl radicals which can abstract hydrogen radicals from the PS backbone forming styryl macroradicals of type A, which decompose by β scission, reducing the PS molecular weight. Therefore, the use of styrene in the melt processing of neat PS provides an additional PS degradation mechanism. In addition, it may be caused by the polymerization of styrene with slightly low molecular weight. In contrast, when PS is melt processed using DCP and styrene monomer; however, in the presence of POSS, the styrene monomer may still combine with DCP resulting in a higher amount of styryl A-type macroradicals that could decompose by β scission. However, A-type macroradicals may also combine with POSS to form B-type macroradicals that are more stable than the former, hence minimizing the PS chain scission. Therefore, the use of styrene monomer as a chain transfer agent increases the consumption of A-type macroradicals, reducing the PS chain scission during the melt processing leading to higher M_w values in relation to the analogous PS-POSS hybrid nanocomposite melt processed in the absence of styrene monomer. Briefly, the PS chain scission that occurs during the reactive melt processing of PS-POSS nanocomposites as a consequence of the free radical initiation can be avoided by the use of styrene monomer as a chain transfer agent.

The increase in the relative amount of hybridized POSS as well as in the molecular weight (M_w) observed with the use of styrene monomer as a chain transfer agent in the synthesis of PS-POSS nanocomposites explains their higher processing torques as compared to the analogous PS-POSS nanocomposites melt processed in the absence of styrene monomer (Table I).

Applied Polymer SCIENCE

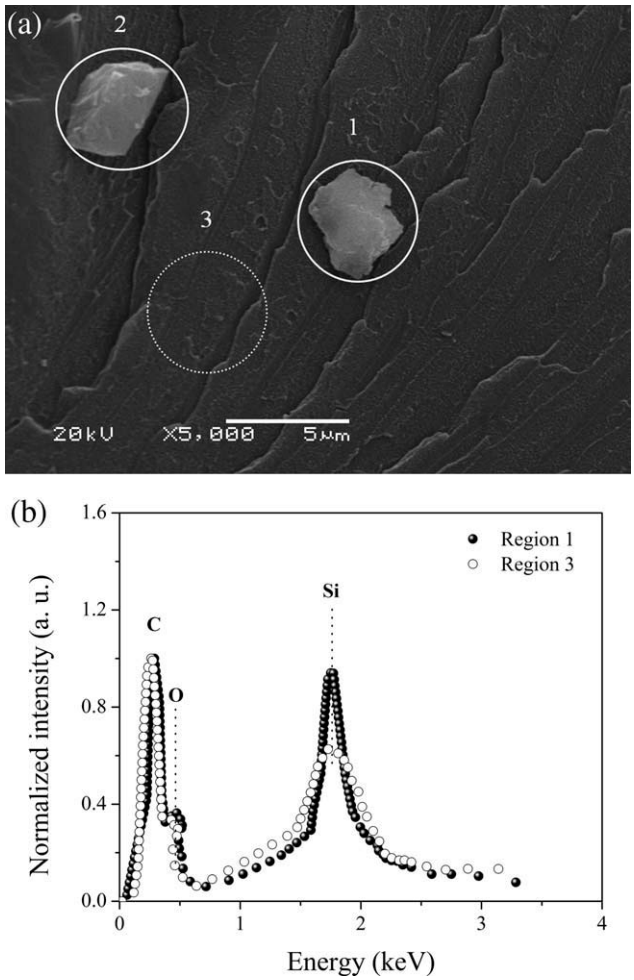

Figure 7. (a) SEM micrograph of the PS-POSS 98/2 sample (DCP/POSS = 0.05; N = 150 rpm; α = 19.6%) and (b) EDS spectra of regions marked 1 and 3 on SEM micrograph.

The use of styrene monomer and other chemicals as chain transfer agents in the modification of polymers through reactive melt processing has been explored in other systems.[51,55–59] For instance, chemical modification of PP with maleic anhydride (MAH) assisted by styrene results in a higher degree of MAH incorporation and lower PP chain scission.[55,58]

PS-POSS materials showed polidispersity index (M_w/M_n) in the range of 1.8–2.2, and no correlation with processing conditions was observed. Indeed, it is difficult to establish this type of correlation since many reactions occur in the reactive processing of PS-POSS.

PS-POSS Morphology

Morphological analyses of PS-POSS materials showed microscale crystalline POSS aggregates and nanoscale POSS clusters and particles dispersed in the PS matrix.

Figure 7(a) shows an SEM micrograph of the PS-POSS 98/2 (DCP/POSS = 0.05; N = 150 rpm; α = 19.6%) representing the general behavior of the PS-POSS materials. SEM micrograph reveals microscale POSS agglomerates (regions marked 1 and 2 on the SEM micrograph) dispersed in the PS matrix. The presence of the elements Si and O in the EDS spectrum of region marked 1 [Figure 7(b)] confirms that it is indeed POSS. EDS spectrum of the region marked 3 [Figure 7(b)] shows the presence of the elements Si and O with no visible POSS aggregates, thus evidencing submicrometer POSS dispersion in the PS-POSS materials.

TEM was used to investigate the submicrometer dispersion of POSS within the PS matrix in the PS-POSS hybrid nanocomposites. Figure 8(a–f) shows representative TEM micrographs of PS-POSS samples processed under different conditions. Figures 8(a–c) show, respectively, the micrographs of PS-POSS 98/2 samples (DCP/POSS = 0.05) processed at 100, 150, and 200 rpm. The α_{POSS} values for these samples are, respectively, 12.3, 19.6, and 26.5%. Figure 8(d) shows the micrograph of the PS-POSS 98/2 with 32.1 wt % of POSS hybridization, processed with 2 wt % of styrene monomer at 200 rpm and with DCP/POSS = 0.05. These micrographs show POSS dispersion within the PS matrix at the nanoscale level. One can observe two populations of POSS clusters with different sizes. A major volume of POSS appears as clusters of 100–200 nm. A high magnification micrograph of sample (a) [Figure 8(e)] revealed that these clusters are formed by POSS primary particles with spherical shape and sizes smaller than 10 nm. A minor volume of POSS appears as smaller clusters of a few POSS particles or even as individual particles.

The PS-POSS morphology, that is, a mixture of microscale POSS aggregates and nanoscale POSS clusters and particles, has been observed for other POSS-containing polymer nanocomposites such as polycarbonate/POSS,[8] PP-g-MA/POSS,[60] and HDPE/EVA/POSS.[61] The dispersion level of POSS in polymer systems is essentially dependent on the compatibility between POSS molecules and polymer main-chain segments. Studies[26,61,62] have shown that the critical minimum concentration at which the POSS tends to remain as separate domains is ~2 wt %, which explains the phase separation occurring in the PS-POSS materials under study. Monticelli et al.[27] have shown that the reactivity between POSS and the polymer matrix is essential to attain a nanostructured material.

The morphology of PS-POSS hybrid nanocomposites melt blended under different conditions was further investigated by small-angle X-ray scattering (SAXS). Figure 9(a) shows the SAXS profiles for PS-POSS with 1–5 wt % of POSS (DCP/POSS = 0.05) processed at a rotor speed of 200 rpm. Figure 9(b) shows the SAXS profiles for PS-POSS with 1–5 wt % of POSS (DCP/POSS = 0.05) processed at a rotor speed of 200 rpm with 2 wt % of styrene as a chain transfer agent. Figure 9(c) shows the SAXS profiles for PS-POSS with 2 wt % of POSS (DCP/POSS = 0.05) processed at rotor speeds of 100, 150, and 200 rpm with and without styrene. There was a good fit between the values obtained applying eq. (8) and the experimental SAXS data, with a correlation coefficient of 0.99. Note that higher order diffraction peaks were not observed in the SAXS experiments, which indicates that the array of POSS aggregates/particles has only a short-range (or local) order in PS/POSS hybrid nanocomposites.

The interface thickness (t), specific interfacial area (S/V), and Porod inhomogeneity lengths (l_p) of the PS-POSS

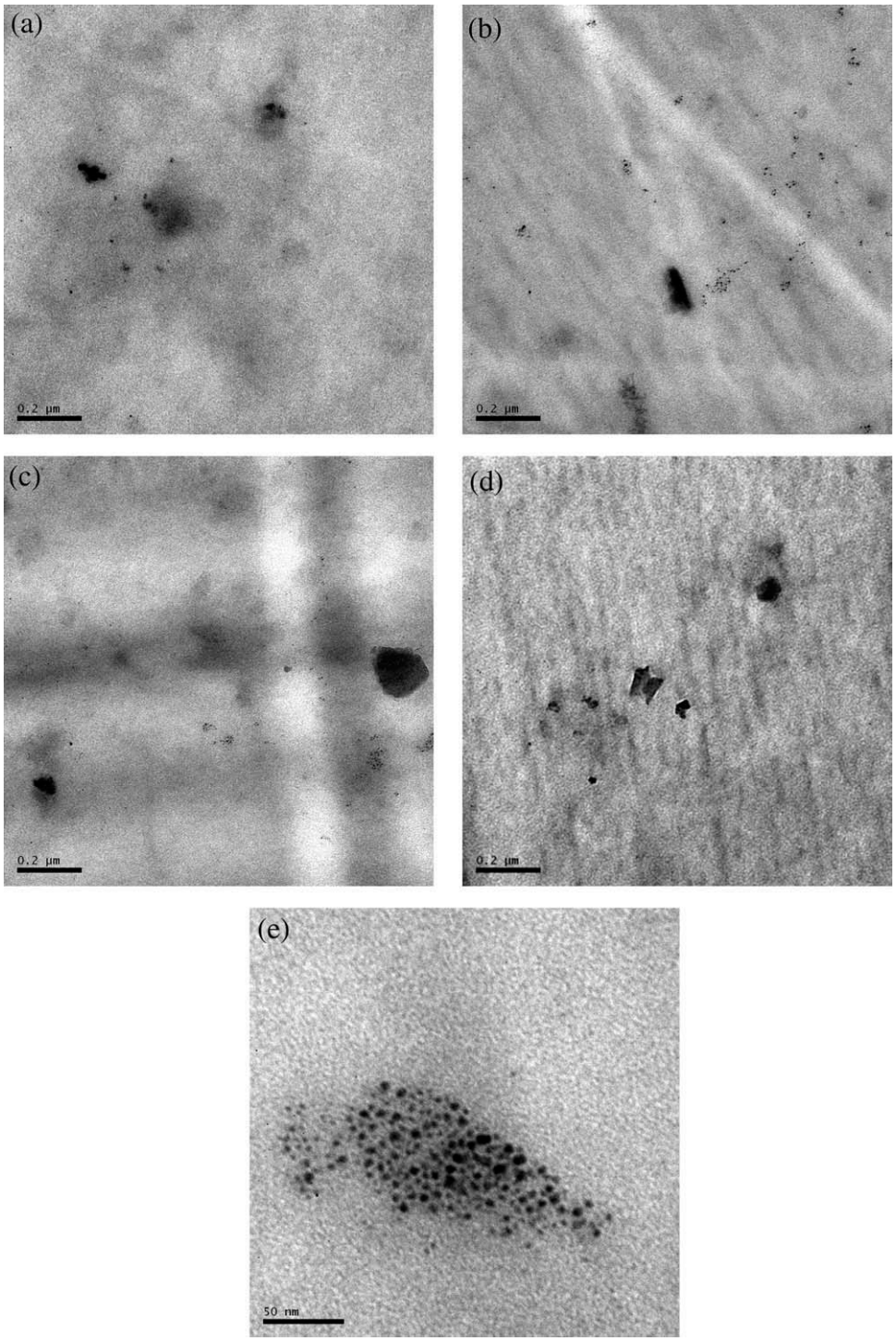

Figure 8. TEM micrographs of PS-POSS hybrid nanocomposites with varying conversion degrees obtained under different processing conditions: (a) PS-POSS 98/2 with $\alpha = 12.3\%$ (DCP/POSS = 0.05; $N = 100$ rpm), (b) PS-POSS 98/2 with $\alpha = 19.6\%$ (DCP/POSS = 0.05; $N = 150$ rpm), (c) PS-POSS 98/2 with $\alpha = 26.5\%$ (DCP/POSS = 0.05; $N = 200$ rpm), (d) PS-POSS 98/2 with $\alpha = 32.1\%$ (DCP/POSS = 0.05; 2 wt % styrene monomer; $N = 200$ rpm), and (e) higher magnification of sample a.

nanocomposites were determined from the SAXS profiles according to the procedure described in the experimental section.

Figure 10 shows the interface thickness (t) for the PS-POSS hybrid nanocomposites containing 1–5 wt % of POSS (DCP/POSS = 0.05), processed at different rotor speeds, with and without styrene monomer. The PS/POSS systems had an interface thickness (t) of ~5–6 nm, which was found to be dependent on the POSS content, rotor speed and the presence of the chain transfer agent (styrene monomer) in the processing. PS/

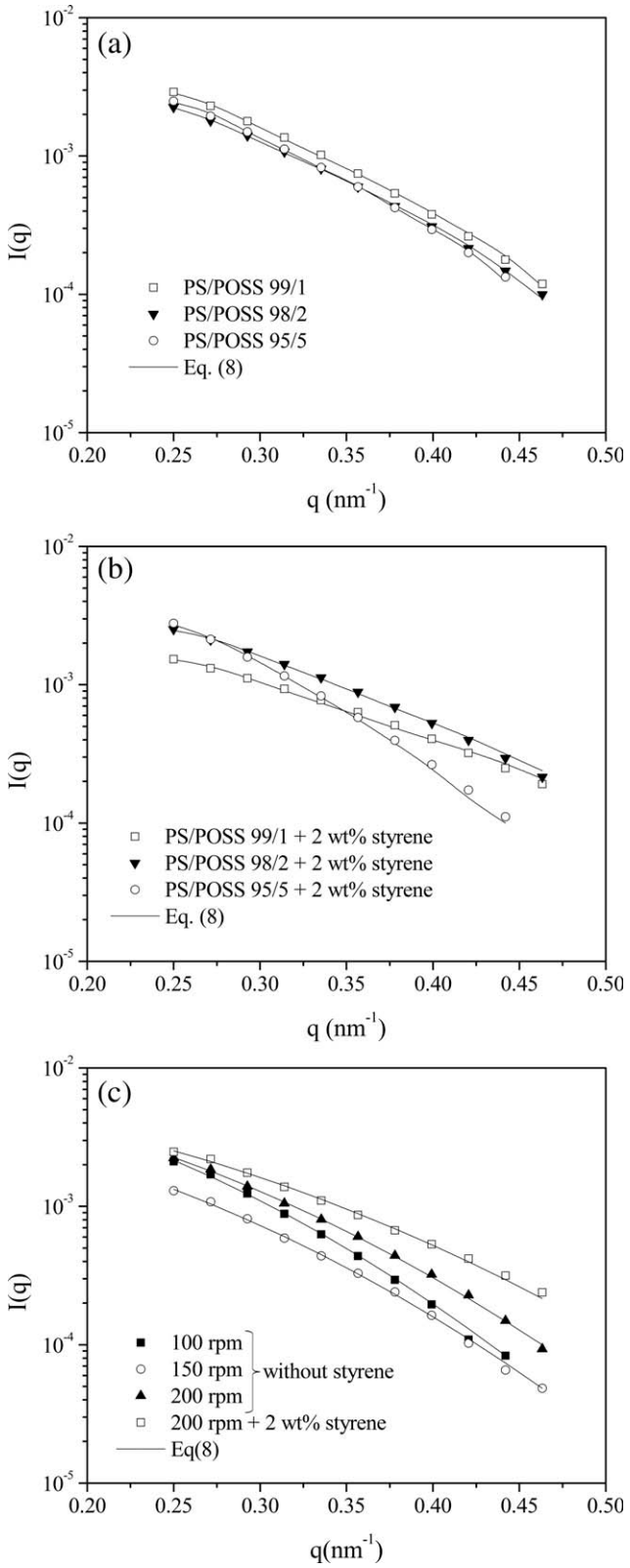

Figure 9. SAXS profiles for PS-POSS hybrid nanocomposites: (a) PS-POSS with 1–5 wt % of POSS (DCP/POSS = 0.05) processed at 200 rpm, (b) PS-POSS with 1–5 wt % of POSS (DCP/POSS = 0.05) processed at 200 rpm with 2 wt % of styrene, and (c) PS-POSS with 2 wt % of POSS (DCP/POSS = 0.05) processed at 100–200 rpm with and without styrene.

POSS hybrid nanocomposites containing higher POSS contents showed thicker interfaces. Although the degree of POSS hybridization is higher for nanocomposites with higher POSS content [Figures 4(a) and 6(a)], there is a larger amount of nonreacted POSS [Figures 4(b) and 6(b)], which probably remains as microscale POSS agglomerates (Figure 7), compared to the hybrids containing lower POSS content. This increases the POSS surface roughness and thus the PS-POSS interface thickness. PS-POSS hybrid nanocomposites with 1–5 wt % of POSS processed with styrene monomer (chain transfer agent) showed lower interface thickness values compared to the analogous PS-POSS nanocomposites processed without styrene monomer. The processing of PS-POSS assisted by styrene increases the degree of POSS hybridization [Figure 6(a)], leading to POSS disaggregation, resulting in smaller PS-POSS interface thicknesses. The PS-POSS processed at higher rotor speeds showed smaller interfacial thicknesses, which is consistent with the higher degree of POSS hybridization achieved [Figures 4(a) and 6(a)]. In summary, for hybrid PS-POSS nanocomposites with improved PS-POSS dispersion, that is, with a greater amount of hybridized and lower amount of nonreacted POSS, those processed at higher rotor speeds and those processed with the aid of a chain transfer agent (styrene monomer) showed smaller interface thickness (t) values.

Interface thickness values of the same order were obtained for PS/silica nanocomposites by Yanagioka et al. using SAXS analysis[36] and by Mortezaei et al. using viscoelastic measurements.[63]

Figure 11 shows the Porod inhomogeneity length (l_p) of PS-POSS hybrid nanocomposites containing 1–5 wt % of POSS (DCP/POSS = 0.05), processed at different rotor speeds, with and without styrene monomer added. The l_p value in PS-POSS is inversely proportional to the average POSS domain sizes. Therefore, PS-POSS materials with enhanced POSS dispersion, that is, with shorter POSS domains, are expected to show higher l_p values. The l_p values in the PS-POSS hybrid nanocomposites were found to be dependent on the POSS content, rotor

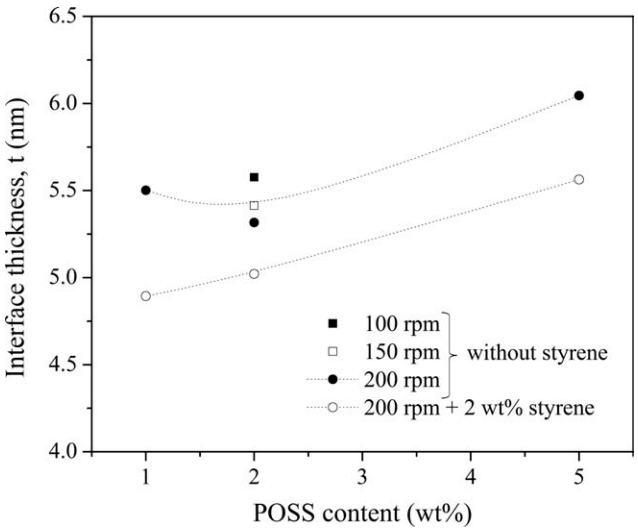

Figure 10. Interface thickness (t) of PS-POSS hybrid nanocomposites containing 1–5 wt % of POSS (DCP/POSS = 0.05), processed at different rotor speeds, with and without styrene monomer (chain transfer agent).

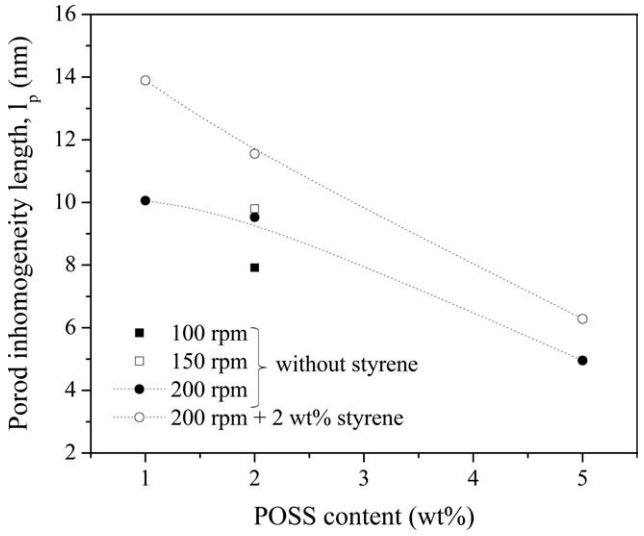

Figure 11. Porod inhomogeneity length (l_p) of PS-POSS hybrid nanocomposites containing 1–5 wt % of POSS (DCP/POSS = 0.05), processed at different rotor speeds, with and without styrene monomer (chain transfer agent).

speed, and the presence or absence of the chain transfer agent (styrene monomer) in the processing. PS/POSS hybrid nanocomposites containing higher POSS contents showed lower l_p values; the increase in the POSS content increases the amount of nonreacted POSS [Figures 4(b) and 6(b)] increasing the tendency of POSS to remain as agglomerates, leading to shorter Porod inhomogeneity lengths (l_p). PS-POSS hybrid nanocomposites with 1–5 wt % of POSS processed with styrene monomer (chain transfer agent) showed longer Porod inhomogeneity lengths (l_p), when compared with the analogous PS-POSS nanocomposites processed without styrene monomer. The processing of PS-POSS assisted by styrene increases the degree of POSS hybridization [Figure 6(a)], leading to POSS disaggregation, resulting in higher l_p values. PS-POSS processed at higher rotor speeds showed longer Porod inhomogeneity lengths (l_p), which is consistent with the higher degrees of POSS hybridization achieved [Figures 4(a) and 6(a)].

The crystalline structure of the POSS in PS-POSS hybrid nanocomposites melt blended under different conditions was investigated by wide angle X-ray diffraction (WAXD). Figure 12 shows the WAXD patterns for the neat PS, neat POSS and PS/POSS 95/5 hybrid nanocomposites processed at 200 rpm with and without styrene monomer.

Neat PS exhibits a typical amorphous pattern with two wide regions with maximum intensities at 2θ angles of 9.9 and 18.9°. The maximum at a 2θ angle of 18.9° corresponds to the *d*-spacing of 0.46 nm (Bragg law) relative to the average distance between aromatic rings in PS.[64] The maximum at a 2θ angle of 9.9° relates to the average PS inter-chain distance, $<R>$,[64,65] which was calculated as 1.11 nm, according to the eq. (10), where λ is the radiation wavelength:[65]

$$< R >= \frac{5}{8}\left(\frac{\lambda}{\sin\theta_{max}}\right) \quad (10)$$

Neat POSS exhibits a typical high crystalline pattern with a strong maximum intensity at a 2θ angle of 7.6°, corresponding to a distance between adjacent lattice planes (d-spacing) of 1.15 nm, according to the Bragg's law. A similar diffraction pattern has been shown for other POSS samples with similar structures.[10,54,66]

PS-POSS materials show WAXD patterns similar to neat PS. The maximum values for the average distance between aromatic rings in PS (2θ = 18.9°; *d*-spacing = 0.46 nm) were unchanged in the PS-POSS materials. PS-POSS 95/5 processed without styrene monomer showed an average PS inter-chain distance ($<R>$ = 1.15 nm) similar to that of neat PS. For the PS-POSS 95/5 processed in the presence of styrene monomer, the maximum average inter-chain distance was shifted to lower 2θ angles, leading to a higher average PS inter-chain distance ($<R>$ = 1.19 nm). The increase in the average PS inter-chain distance can be understood as an increase in the packing length, defined as the occupied volume of a chain divided by the mean-square end-to-end distance, caused by POSS hybridization onto the PS chain. The fact that WAXD patterns of PS-POSS do not show the POSS diffraction peaks should indicate, in principle, the disappearance of the POSS crystalline structure in the PS-POSS materials. The interactions between POSS and PS caused by the PS-POSS hybridization would contribute to the disruption of the crystalline structure of POSS in the PS-POSS materials; in fact, this interaction would broaden the POSS signals due to a loss of regularity in relation to the neat POSS crystals. However, the presence of micrometric aggregates of POSS in the SEM micrograph [Figure 7(a)] provides evidence to support the existence of crystalline POSS domains in the PS-POSS materials, in addition to amorphous POSS clusters and particles. Moreover, the high melting point of phenyl-POSS, ~550°C,[67] well above the processing temperature (200–210°C), is a factor that would contribute to maintaining the crystalline structure of POSS in the PS-POSS materials. On the other

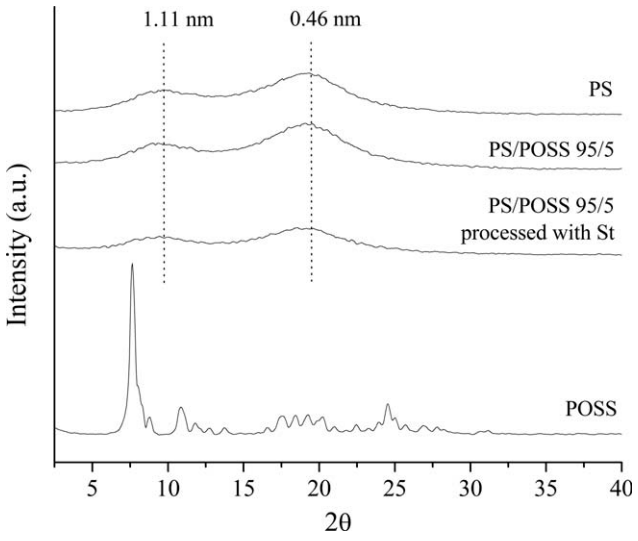

Figure 12. WAXD patterns of neat PS, neat POSS, and PS/POSS 95/5 hybrid nanocomposites processed at 200 rpm with and without styrene monomer.

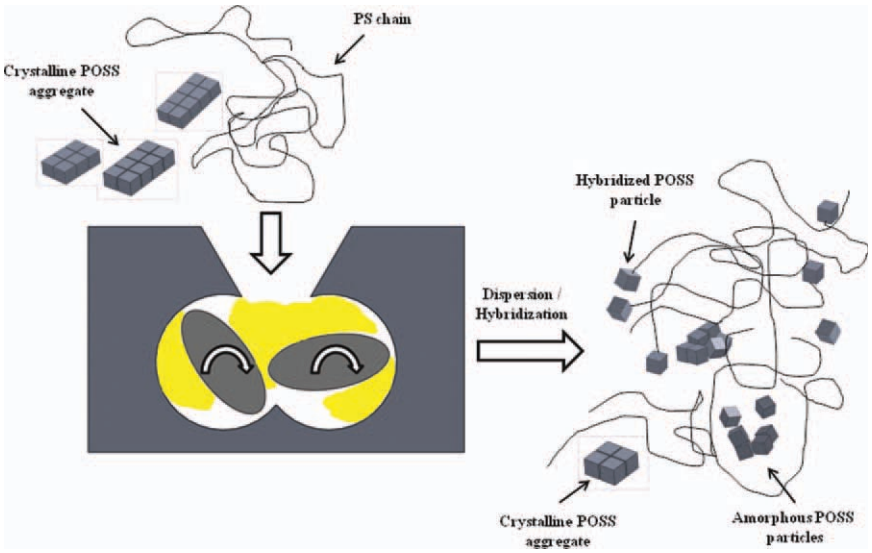

Figure 13. Schematic representation of POSS dispersion state in the PS/POSS hybrid nanocomposites obtained by reactive melt blending. [Color figure can be viewed in the online issue, which is available at wileyonlinelibrary.com.]

hand, because the POSS content is low (5 wt %) in these PS-POSS materials, there is a possibility that the POSS signals were obscured by the amorphous halo of the PS matrix. Sánchez-Soto et al.[8] have shown that the POSS diffraction peaks are not visible in the WAXD pattern for a PC/phenyl-POSS nanocomposite containing 2.5 wt % of POSS and that they become more visible for nanocomposites containing above 10 wt % of POSS. They attributed this behavior to the increased interaction of the polymer matrix for nanocomposites with a low concentration of POSS. The maintenance of the crystalline structure of the POSS in polymer systems has been shown for reactive melt grafted PP/POSS systems,[26] in melt blended HDPE/EVA/POSS[61] and in *in situ* polymerized PS/styryl-POSS systems.[30]

Figure 13 shows a schematic representation of the POSS dispersion state in the PS/POSS hybrid nanocomposites obtained by reactive melt blending in this study. Three levels of POSS dispersion are shown: individual POSS particles covalently bonded to the PS chain (hybridized POSS particles), nonreacted crystalline POSS aggregates and nonreacted amorphous POSS clusters. As shown earlier, the POSS dispersion level is dependent on the PS-POSS processing conditions, namely the POSS content, rotor speed, and presence of the chain transfer agent (styrene monomer) in the processing. PS-POSS hybrid nanocomposites with a higher amount of hybridized POSS, processed at higher mixing intensity and with the assistance of styrene monomer showed enhanced POSS dispersion.

PS-POSS Viscoelastic Properties

The viscoelastic properties of PS-POSS hybrid nanocomposites processed under different conditions were evaluated by dynamical mechanical analysis (DMA). DMA curves of the storage modulus (E') and tan δ versus temperature for PS-POSS samples containing 0–5 wt % of POSS (DCP/POSS = 0.05) processed at a rotor speed of 200 rpm with and without styrene monomer (chain transfer agent) are shown, respectively, in Figure 14(a,b). The glass transition temperature (T_g) in the range

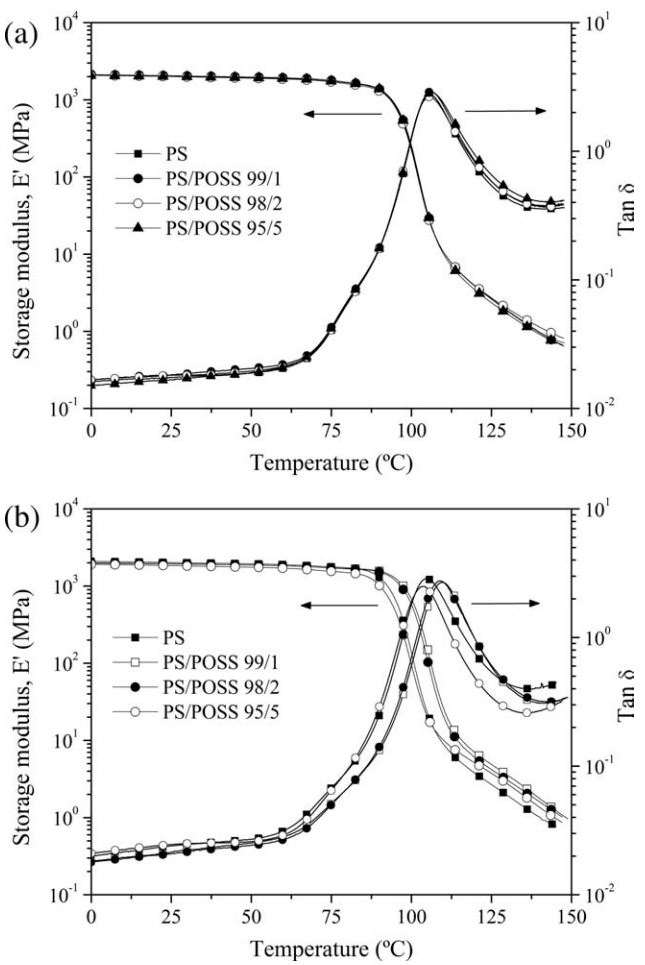

Figure 14. DMA curves of storage modulus and tan δ versus temperature for PS/POSS hybrid nanocomposites with 0–5 wt % of POSS (DCP/POSS = 0.05) melt blended at a rotor speed of 200 rpm without styrene monomer (a) and with styrene monomer as a chain transfer agent (b).

of 100–110°C and β relaxation in the range of 10–50°C of PS were monitored. The T_g (α relaxation) of PS has been assigned to PS long-range chain motions whereas β relaxation has been assigned to phenyl group torsional vibration[68] or fluctuations of helices or parts of them.[69,70] In fact, the origin of the β relaxation of PS remains a controversial issue. It has also been observed for other polymers with phenyl rings in the backbone[71,72] or as side-chain groups.[73]

The storage moduli of PS-POSS materials below the T_g were practically similar to that of neat PS. Indeed, nanofillers with low aspect ratio like cubic-shaped POSS at low loadings (up to 5 wt %) are not expected to affect significantly the stiffness of polymeric matrixes.[74,75] However, it is difficult to ascribe this behavior only to the POSS loading since PS-POSS materials show different POSS hybridization degrees and POSS particle sizes and different average molecular weights.

For the PS-POSS materials obtained by reactive melt blending without the use of the chain transfer agent (styrene monomer) [Figure 14(b)], the T_g and β relaxation were similar to those of neat PS.

On the other hand, although for PS-POSS materials melt blended with the assistance of styrene monomer as a chain transfer agent [Figure 14(b)] the β relaxations were also similar to that of neat PS, the T_g relaxation was shifted. PS-POSS materials containing 1 and 2 wt % of POSS showed an increase in T_g from 105°C (neat PS) to 109°C, based on the tan δ maximum. In contrast, PS-POSS materials containing 5 wt % of POSS showed a T_g of 104°C, that is, a reduction of 1°C in relation to neat PS, based on the tan δ maximum.

As discussed earlier, these materials show different POSS hybridization degrees [Figure 6(a)], different amounts of nonreacted POSS [Figure 6(b)], and different average molecular weights [Figure 6(b)]. The differences in the molecular weights of these materials are not expected to affect the T_g, since the average molecular weights are above the critical value for PS, that is, 100,000 g mol^{-1} [76]. The observed shifts in T_g for the PS/POSS hybrid nanocomposites melt blended with the addition of styrene monomer [Figure 13(b)] are due to the difference in the amounts of nonreacted and hybridized POSS of each material, that is, T_g for PS-POSS is dependent on the level of POSS dispersion in each material.

For the PS/POSS hybrid nanocomposites containing 1 and 2 wt % of POSS, the increase in T_g [Figure 14(b)] can be related to the restricted chain mobility caused by the POSS hybridized to the PS chain [Figure 6(a)]. For the PS/POSS hybrid nanocomposite containing 5 wt % of POSS, although the amount of PS-POSS hybrids is larger, there is also a larger amount of nonreacted POSS [Figure 6(b)], as compared to the materials with 1 and 2 wt % of POSS. The nonreacted POSS agglomerates increase the free volume decreasing the molecular weight between entanglements and therefore the chain mobility, reducing the T_g of PS. Similar behavior was reported by Monticelli et al. in PSMA/POSS systems[27] and for other POSS-containing polymer systems.[1,77–80] Cardoen and Coughlin[81] observed no change in T_g for hemi-telechelic PS-POSS copolymers, as compared to the neat PS. They attributed this behavior to the fact that POSS is tethered at the end of the PS chains in these materials, which isolates the POSS moieties and PS chains from each other, causing no change in the PS T_g. This effect must be also considered since both types of PS-POSS hybridization, that is, graft and end-chain, may occur in the PS-POSS materials under study, according to the reaction scheme in Figure 3.

CONCLUSION

The synthesis of PS-POSS hybrid nanocomposites by reactive melt blending of PS and POSS was performed in a mixing chamber of a torque rheometer under different processing conditions. DCP was used as a free radical initiator and styrene monomer as a chain transfer agent. The effects of the processing conditions, namely the mixing intensity and the amounts of POSS, DCP, and styrene monomer in the molecular structure, and the morphology of the PS-POSS hybrid nanocomposites were investigated.

The degree of POSS hybridization (α_{POSS}) was shown to increase with the POSS content, DCP/POSS ratio, and rotor speed. For the PS-POSS materials processed in the absence of the chain transfer agent (styrene monomer) the increase in α_{POSS} occurs at the expense of decreased molecular weight, that is, PS chain scission occurs simultaneously with POSS hybridization during the reactive melt blending. However, we have shown that the use of styrene monomer as a chain transfer agent in the synthesis of PS-POSS hybrid materials enhances the α_{POSS} value and avoids the PS chain degradation as a consequence of the free radical initiation. POSS hybridization degrees of up to 40 wt % were achieved with the use of styrene monomer in the synthesis of PS-POSS. Styrene monomer acts by reducing the steric hindrance in relation to the hybridization reaction between the POSS and the PS chains.

The PS-POSS morphology comprises nanoscale POSS clusters and particles and microscale crystalline POSS aggregates. PS-POSS with higher α_{POSS} and lower amounts of nonbounded POSS showed improved POSS dispersion, characterized by smaller interfacial thickness (t) and greater Porod inhomogeneity lengths (l_p).

The correlations between the processing conditions, molecular structure, and morphology observed in this study allow the POSS dispersion level in the PS-POSS materials to be tuned by controlling the reactive melt blending through the choice of the processing conditions. These insights are very useful for the development of PS-POSS materials with optimized performance. Moreover, they can be extended to other POSS-containing polymer systems.

ACKNOWLEDGMENTS

The authors are grateful to CNPq, Brazil for financial support, CME-UFRGS for the TEM analysis, and the Brazilian Synchrotron Light Laboratory (LNLS) for the SAXS analysis.

REFERENCES

1. Hao, N.; Boehning, M.; Schoenhals, A. *Macromolecules* **2007,** *40*, 9672.

2. Thompson, A.; Bianchi, O.; Amorim, C. L. G.; Lemos, C.; Teixeira, S. R.; Samios, D.; Giacomelli, C.; Crespo, J. S.; Machado, G. *Polymer* **2011,** *52*, 1037.
3. Gnanasekaran, D.; Madhavan, K.; Reddy, B. S. R. *J. Sci. Ind. Res.* **2009,** *68*, 437.
4. Pielichowski, K.; Njuguna, J.; Janowski, B.; Pielichowski, J. In Supramolecular Polymers Polymeric Betains Oligomers; Abe, A.; Dusek, K.; Kobayashi, S., Eds.; Springer-Verlag: Berlin, **2006.**
5. Dal Castel, C.; Bianchi, O.; Oviedo, M. A. S.; Liberman, S. A.; Mauler, R. S.; Oliveira, R. V. B. *Mater. Sci. Eng. C* **2009,** *29*, 602.
6. Herman Teo, J. K.; Teo, K. C.; Pan, B.; Xiao, Y.; Lu, X. *Polymer* **2007,** *48*, 5671.
7. Mather, P. T.; Jeon, H. G.; Romo-Uribe, A.; Haddad, T. S.; Lichtenhan, J. D. *Macromolecules* **1999,** *32*, 1194.
8. Sánchez-Soto, M.; Schiraldi, D. A.; Illescas, S. *Eur. Polym. J.* **2009,** *45*, 341.
9. Li, G. Z.; Wang, L. C.; Ni, H. L.; Pittman, C. U. *J. Inorg. Organomet. Polym.* **2001,** *11*, 123.
10. Zhao, Y. Q.; Schiraldi, D. A. *Polymer* **2005,** *46*, 11640.
11. Fina, A.; Tabuani, D.; Carniato, F.; Frache, A.; Boccaleri, E.; Camino, G. *Thermochim. Acta* **2006,** *440*, 36.
12. Silva, R.; Salles, C.; Mauler, R.; Oliveira, R. *Polym. Int.* **2010,** *59*, 1221.
13. Misra, R.; Alidedeoglu, A. H.; Jarrett, W. L.; Morgan, S. E. *Polymer* **2009,** *50*, 2906.
14. Hirai, T.; Leolukman, M.; Jin, S.; Goseki, R.; Ishida, Y.; Kakimoto, M.-A.; Hayakawa, T.; Ree, M.; Gopalan, P. *Macromolecules* **2009,** *42*, 8835.
15. Yang, B.; Xu, H.; Wang, J.; Gang, S.; Li, C. *J. Appl. Polym. Sci.* **2007,** *106*, 320.
16. Zheng, L.; Kasi, R. M.; Farris, R. J.; Coughlin, E. B. *J. Polym. Sci. Polym. Chem.* **2002,** *40*, 885.
17. Fabris, F. W.; Stedile, F. C.; Mauler, R. S.; Nachtigall, S. M. B. *Eur. Polym. J.* **2004,** *40*, 1119.
18. Fu, B. X.; Lee, A.; Haddad, T. S. *Macromolecules* **2004,** *37*, 5211.
19. Huang, Y.; Peng, H.; Lam, J. W. Y.; Xu, Z.; Leung, F. S. M.; Mays, J. W.; Tang, B. Z. *Polymer* **2004,** *45*, 4811.
20. Ohno, K.; Sugiyama, S.; Koh, K.; Tsujii, Y.; Fukuda, T.; Yamahiro, M.; Oikawa, H.; Yamamoto, Y.; Ootake, N.; Watanabe, K. *Macromolecules* **2004,** *37*, 8517.
21. Passaglia, E.; Coiai, S.; Ricci, L.; Ciardelli, F. *Macromol. Symp.* **2004,** *218*, 61.
22. Shockey, E. G.; Bolf, A. G.; Jones, P. F.; Schwab, J. J.; Chaffee, K. P.; Haddad, T. S.; Lichtenhan, J. D. *Appl. Organomet. Chem.* **1999,** *13*, 311.
23. Patel, R. R.; Mohanraj, R., Jr.; Pittman, C. U. *J. Polym. Sci. Part B Polym. Phys.* **2006,** *44*, 234.
24. Xanthos, M. Reactive Extrusion: Principles and Practice; Hanser: Munich, **1992.**
25. Janssen, L. P. B. Reactive Extrusion Systems; Marcel Dekker: New York, **2004.**
26. Zhou, Z.; Cui, L.; Zhang, Y.; Zhang, Y.; Yin, N. *Eur. Polym. J.* **2008,** *44*, 3057.
27. Monticelli, O.; Fina, A.; Ullah, A.; Waghmare, P. *Macromolecules* **2009,** *42*, 6614.
28. Yan Song, X.; Ping Geng, H.; Li, Q. F. *Polymer* **2006,** *47*, 3049.
29. Wu, J.; Haddad, T. S.; Mather, P. T. *Macromolecules* **2009,** *42*, 1142.
30. Zhang, H.-X.; Lee, H.-Y.; Shin, Y.-J.; Yoon, K.-B.; Noh, S.-K.; Lee, D.-H. *Polym. Int.* **2008,** *57*, 1351.
31. Grcev, S.; Schoenmakers, P.; Iedema, P. *Polymer* **2004,** *45*, 39.
32. Bianchi, O.; Repenning, G. B.; Canto, L. B.; Mauler, R. S.; Oliveira, R. V. B. *Polimeros* **2012,** *22*, 125.
33. Pyun, J.; Matyjaszewski, K. *Macromolecules* **2000,** *33*, 217.
34. Bevington, J. C.; Huckerby, T. N. *Eur. Polym. J.* **2006,** *42*, 1433.
35. Vonk, C. *J. Appl. Crystallogr.* **1978,** *11*, 541.
36. Yanagioka, M.; Toney, M. F.; Frank, C. W. *Macromolecules* **2009,** *42*, 1331.
37. Svergun, D. I. Structure Analysis by Small-Angle X-Ray and Neutron Scattering; Plenum Press: New York, **1987.**
38. Porod, G. In Small Angle X-ray Scattering; Glatter, O.; Kratky, O., Eds.; Academic Press: London, **1981.**
39. Ruland, W. *J. Appl. Crystallogr.* **1971,** *4*, 70.
40. Koberstein, J. T.; Morra, B.; Stein, R. S. *J. Appl. Crystallogr.* **1980,** *13*, 34.
41. Perrin, P.; Prud'homme, R. E. *Macromolecules* **1994,** *27*, 1852.
42. Vonk, C. *J. Appl. Crystallogr.* **1971,** *4*, 340.
43. Vonk, C. *J. Appl. Crystallogr.* **1973,** *6*, 81.
44. Todo, A.; Hashimoto, T.; Kawai, H. *J. Appl. Crystallogr.* **1978,** *11*, 558.
45. Hashimoto, T.; Fujimura, M.; Kawai, H. *Macromolecules* **1980,** *13*, 1660.
46. Sheng, J.; Hu, J.; Yuan, X.-B.; Han, Y.-P.; Li, F.-K.; Bian, D.-C. *J. Appl. Polym. Sci.* **1998,** *70*, 805.
47. Hashimoto, T.; Shibayama, M.; Kawai, H. *Macromolecules* **1980,** *13*, 1237.
48. Levenberg, K. *Quart. Appl. Math.* **1944,** *2*, 164.
49. Marquardt, D. W. *J. Soc. Ind. Appl. Math.* **1963,** *11*, 431.
50. Kim, J.-E.; Zin, W.-C.; Ahn, J.-H. *Eur. Polym. J.* **2009,** *45*, 2450.
51. Moad, G. *Prog. Polym. Sci.* **1999,** *24*, 81.
52. Nachtigall, S. M. B.; Stedile, F. C.; Felix, A. H. O.; Mauler, R. S. *J. Appl. Polym. Sci.* **1999,** *72*, 1313.
53. Tsuchida, A.; Bolln, C.; Sernetz, F. G.; Frey, H.; Mülhaupt, R. *Macromolecules* **1997,** *30*, 2818.
54. Zheng, L.; Hong, S.; Cardoen, G. G.; Burgaz, E.; Gido, S. P.; Coughlin, E. B. *Macromolecules* **2004,** *37*, 8606.
55. Bettini, S. H. P.; Ruvolo, A. C. *J. Appl. Polym. Sci.* **2008,** *107*, 1430.
56. Díaz, M. F.; Barbosa, S. E.; Capiati, N. J. *J. Appl. Polym. Sci.* **2009,** *114*, 3081.

57. Xue, F.; Takeda, D.; Kimura, T.; Minabe, M. *Polym. Degrad. Stabil.* **2004,** *83*, 461.
58. Li, Y.; Xie, X.-M.; Guo, B.-H. *Polymer* **2001,** *42*, 3419.
59. Passaglia, E.; Coiai, S.; Augier, S. *Prog. Polym. Sci.* **2009,** *34*, 911.
60. Fina, A.; Tabuani, D.; Peijs, T.; Camino, G. *Polymer* **2009,** *50*, 218.
61. Scapini, P.; Figueroa, C. A.; Amorim, C. L. G.; Machado, G.; Mauler, R. S.; Crespo, J. S.; Oliveira, R. V. B. *Polym. Int.* **2010,** *59*, 175.
62. Fina, A.; Monticelli, O.; Camino, G. *J. Mater. Chem.* **2010,** *20*, 9297.
63. Mortezaei, M.; Farzi, G.; Kalaee, M. R.; Zabihpoor, M. *J. Appl. Polym. Sci.* **2011,** *119*, 2039.
64. Wu, J.; Haddad, T. S.; Kim, G. M.; Mather, P. T. *Macromolecules* **2007,** *40*, 544.
65. Halasa, A. F.; Wathen, G. D.; Hsu, W. L.; Matrana, B. A.; Massie, J. M. *J. Appl. Polym. Sci.* **1991,** *43*, 183.
66. Yoon, K. H.; Polk, M. B.; Park, J. H.; Min, B. G.; Schiraldi, D. A. *Polym. Int.* **2005,** *54*, 47.
67. Brown, J. F.; Vogt, L. H.; Prescott, P. I. *J. Am. Chem. Soc.* **1964,** *86*, 1120.
68. Sperling, L. H. Introduction to Physical Polymer Science, 4th ed.; Wiley: Hoboken, **2006.**
69. Lupascu, V.; Picken, S. J.; Wübbenhorst, M. *Macromolecules* **2006,** *39*, 5152.
70. Lupascu, V.; Picken, S. J.; Wübbenhorst, M. *J. Non-Cryst. Solids* **2006,** *352*, 5594.
71. Pratt, G. J.; Smith, M. J. A. *Polym. Int.* **1997,** *43*, 137.
72. Hardy, L.; Stevenson, I.; Fritz, A.; Boiteux, G.; Seytre, G.; Schönhals, A. *Polymer* **2003,** *44*, 4311.
73. Fritz, A.; Schönhals, A.; Sapich, B.; Stumpe, J. *Macromol. Chem. Phys.* **1999,** *200*, 2213.
74. Romero-Guzmán, M. E.; Romo-Uribe, A.; Zarate-Hernandez, B. M.; Cruz-Silva, R. *Rheol. Acta* **2009,** *48*, 641.
75. Martins, J. N.; Bassani, T. S.; Oliveira, R. V. B. *Mater. Sci. Eng. C* **2012,** *32*, 146.
76. Masuda, T.; Kitagawa, K.; Inoue, T.; Onogi, S. *Macromolecules* **1970,** *3*, 116.
77. Xu, H.; Kuo, S.-W.; Lee, J.-S.; Chang, F.-C. *Polymer* **2002,** *43*, 5117.
78. Xu, H.; Kuo, S.-W.; Lee, J.-S.; Chang, F.-C. *Macromolecules* **2002,** *35*, 8788.
79. Kopesky, E. T.; Haddad, T. S.; McKinley, G. H.; Cohen, R. E. *Polymer* **2005,** *46*, 4743.
80. Soong, S. Y.; Cohen, R. E.; Boyce, M. C. *Polymer* **2007,** *48*, 1410.
81. Cardoen, G.; Coughlin, E. B. *Macromolecules* **2004,** *37*, 5123.